Dodecanethiol-Protected Copper/Silver Bimetallic Nanoclusters and Their Surface Properties

T. P. Ang[†] and W. S. Chin*

Department of Chemistry, National University of Singapore, 3 Science Drive 3, Singapore 117543

Received: June 23, 2005; In Final Form: September 28, 2005

Dodecanethiol-protected copper/silver bimetallic nanoclusters were prepared by a liquid-phase method using different copper to silver feed ratios. The morphology and size of the prepared nanoclusters were analyzed with X-ray diffraction (XRD) and transmission electron microscopy (TEM), while their spectroscopic and surface properties were characterized by infrared (IR) and X-ray photoelectron spectroscopy (XPS), thermal gravimetric analysis (TGA), differential scanning calorimetry (DSC), and ^{13}C cross-polarization magic angle spinning NMR (^{13}C CPMAS NMR). TEM analysis indicated that all the bimetallic clusters prepared are ∼4−6 nm in size. On the other hand, the results of XRD, XPS, and Fourier transform infrared (FTIR) spectroscopy suggested that the surfaces of the alloy nanoclusters are mostly enriched with the less noble metal copper atoms. This surface enrichment of copper may be attributed to a galvanic exchange process during preparation, and the extent of enrichment is directly related to the copper feed ratio used. Interestingly, DSC studies showed two melting transitions in some of these alloy samples, suggesting different packing behavior of the dodecanethiol chains onto the heterogeneously intercalated silver- and copper-rich surfaces.

Introduction

Bimetallic nanoparticles, in which two kinds of metals are contained in one particle, are more interesting than monometallic nanoparticles largely due to the improved catalytic properties they exihibit.[1,2] Bimetallization can help to improve the catalytic properties of the original single-metal catalysts and, at the same time, creates a new property that cannot be achieved by monometallic catalysts.[2] In addition, bimetallic nanoparticles may also exhibit electronic[3] and optical[4,5] properties that are distinct from those of their monometallic counterparts.

Bimetallic nanoparticles can be synthesized by the simultaneous coreduction of two kinds of metal ions with or without a protecting group (usually a polymer or a surfactant)[6−10] or by the successive reduction of one metal over the nuclei of another.[11−15] Evaporation followed by condensation[16] and laser-induced melting[17−20] are the other two commonly used methods. Depending on the preparation methods used, either the alloy or the core−shell (layered) nanoparticles are produced.

In another aspect, long chain alkanethiols have been found to self-assemble into compact monolayers (i.e., three-dimensional self-assembled monolayers (3D SAMs)) on metallic nanoparticles.[6−8,21] These stable monolayer-protected metal clusters (MPCs) can be readily isolated for further studies and applications. Following Brust's success in preparing thiol-derivatized gold MPCs using the two-phase liquid/liquid systems,[22a] a similar method has also been extended to prepare monolayer-protected gold/silver alloy nanoclusters (MPACs).[6−8,10,15] These MPACs are examples of alloy nanoclusters that can be isolated in dry form. It was found that the metal content in and on the surfaces of the MPAC cores may differ from the feed ratio used for the synthesis of the MPACs.[6,7] In addition, Sandhyarani et al. have shown that superlattices due to interdigitation between MPACs can also be formed.[7]

On the other hand, the preparation of copper MPCs often involves a complication. As our previous study has shown,[23] an undesirable copper thiolates bilayer complex[24] may be produced if the copper to alkanethiol feed ratio is not properly controlled. As such, reports on alkanethiol-protected copper nanoparticles or MPACs are scarce.[15,23,25] In this paper, we present the first report on copper/silver bimetallic nanoclusters using 1-dodecanethiol ($C_{12}H_{25}SH$) as the protecting group. While we have found evidence for the formation of 3D SAMs on the alloy nanoclusters, our analysis results also pointed out differences between the surface compositions and the core particles. Notably, the less noble component (copper) was found to show a higher tendency to occupy the surface of the nanoclusters, probably due to galvanic reaction. In addition, spectroscopic and thermal analysis also suggested that the SAMs formed on the copper- or silver-rich surfaces are slightly different in behavior.

Experimental Section

Materials. Copper(II) nitrate hemipentahydrate (98%) was obtained from Sigma-Aldrich, and 1-dodecanethiol (98%) was from Acros Organic. Silver nitrate (99.8%) was from Merck, and sodium borohydride (96%) was from Fluka. All reagents and solvents were used as received. Milli-Q purified water was used throughout the preparation.

Preparation. The thiolated copper/silver bimetallic nanoclusters were synthesized in solution using a method modified from the literature.[23,26] The entire reaction was purged and carried out in an inert N_2 atmosphere to prevent oxidation of the metals. Suitable amounts of copper(II) nitrate and/or silver nitrate were first dissolved in 120 mL of ethanol in a two-necked round-bottomed flask to make the desired Cu to Ag feed ratio with the total metal ion concentration kept at 0.015 M. Then, a 1:1 molar ratio of 1-dodecanethiol was added with vigorous

* To whom correspondence should be addressed. E-mail: chmcws@nus.edu.sg.

[†] Current address: Institute of Chemical and Engineering Sciences, 1 Pesek Road, Jurong Island, Singapore 627833.

10.1021/jp053429r CCC: $30.25
Published on Web 11/05/2005

stirring. About 80 mL of 0.09 M sodium borohydride in ethanol was then added dropwise into the reaction mixture from a dropping funnel. The reaction mixture was maintained at room temperature with vigorous stirring for 2 h. A dark brownish precipitate was isolated by centrifugation, washed repeatedly with deionized water, toluene, ethanol, and acetone, and then vacuum dried. For comparison, samples with Cu to Ag molar ratios of 1:1, 1:2, 1:3, 2:1, and 3:1 were prepared and the two monometallic samples (i.e., molar ratios 1:0 and 0:1) were also prepared similarly. In addition, a physically mixed sample of the two monometallic clusters was prepared for comparison.

Characterization. The surface chemical composition of the copper nanoclusters was analyzed with X-ray photoelectron spectroscopy (XPS) using a VG Scientific ESCALAB MK II operated at 120 W. A monochromatic Mg Kα X-ray source at 1253.6 eV was used, and the system was calibrated with respect to the Cu 2p peak from a standard sample ($CuSO_4 \cdot 5H_2O$). The crystal phase of the nanoclusters was analyzed using a Siemens X-ray diffactometer (D5005) operated at 40 kV and 40 mA. Solid-state cross-polarization magic angle spinning (CPMAS) ^{13}C NMR spectra were recorded with a Bruker DRX 400 MHz spectrometer with the spin rate of 8000 per second. Fourier transform infrared (FTIR) spectra were recorded on KBr disks using a Bio-rad FTIR spectrometer FTS 165. Ultraviolet/visible absorption spectra were recorded with a Shimadzu UV-2550 spectrophotometer by grinding the sample with Nujol onto filter paper. Elemental analyses were performed using a Thermo Jarrell Ash IRIS AP Duo inductively coupled optical-emission spectrometer and a Perkin-Elmer PE 2400 CHNS elemental analyzer.

The size and morphology of the nanoclusters prepared were determined by transmission electron microscopy (TEM). A drop of nanoclusters dispersed in toluene was placed on a copper grid coated with a thin film of Formvar and dried. Electron micrographs were taken with a JEOL LEM-100CXII electron microscope at an accelerating voltage of 100 kV. The particle sizes were determined from the maximum length of the particles.

The desorption temperature of the adsorbed alkanethiols and the percentage weight loss of the nanoclusters were determined using a TA Instruments SDT 2960 simultaneous DTA-TGA analyzer under nitrogen (flow rate = 70 mL/min) at a heating rate of 20 °C/min. Differential scanning calorimetry (DSC) was performed with a TA Instruments DSC 2920 calorimeter under nitrogen (flow rate = 100 mL/min) at a heating rate of 10 °C/min.

Results and Discussion

To facilitate our discussion, all samples are abbreviated as Cu/Ag(*X*:*Y*), for MPACs that are prepared with an *X*:*Y* copper to silver molar feed ratio. For consistency, the monometallic copper and silver samples are quoted as Cu/Ag(1:0) and Cu/Ag(0:1), respectively. In all samples, the dodecanethiol to total metal ratio is kept at 1:1. We will first investigate the morphological and chemical properties of the MPACs, followed by a closer investigation of the surface content and adsorbed layers on the MPACs by various techniques.

(A) Structural and Morphological Characterization. Figure 1 depicts typical TEM images, together with size distribution histograms, of the different Cu/Ag MPACs prepared. For comparison, TEM micrographs of the monometallic silver and copper samples are also included in Figure 1a and g, respectively.

In general, individual spherical nanoparticles can be seen for all the samples prepared. In some cases, especially for the copper-rich MPACs, larger or aggregated clusters are detected also. The average sizes of the dispersed particles are estimated to be ~4−6 nm by taking the average of at least 100 particles. While the formation of a copper thiolate stoichiometric compound cannot be totally excluded in our preparation, the TEM analysis confirms the formation of MPAC nanoparticles (see the Supporting Information).

It has been pointed out that the average particle size of alloy clusters will depend on the specific metal components used to prepare the MPACs.[6] For example, while Au/Pd MPACs appear to be smaller, the Au/Ag MPACs were found to be larger as compared to the monometallic Au nanoparticles. This observation has been partly attributed to galvanic metal exchange which is responsible for the segregation of the less noble metal component to the surfaces.[6,15] Thus, in our copper-rich samples (i.e., higher copper-to-silver feed ratios), some of the copper seeds formed initially may act as an ancillary reducing agent for Ag^+ present in the solution. Thus, some copper atoms may eventually leach out from the cores to produce copper-enriched surfaces due to a galvanic process. Since it will take two Ag atoms to form for each Cu^{2+} ion released, we expect the average particle size of these Cu/Ag MPACs to be slightly larger than the Cu monometallic clusters. For the silver-rich samples, on the other hand, silver is expected to be reduced first and, thus, more of the copper component is expected to be present on the surfaces.

Figure 2 presents the powdered X-ray diffractograms of the Cu/Ag MPAC samples. It is observed that the Ag(111) peak appears prominently in the spectum of the silver Cu/Ag(0:1) sample but is prevalent only in the silver-rich MPAC samples. On the other hand, peaks due to face-centered cubic (fcc) copper metal are not detected, as is expected for very small copper clusters.[23,27] Instead, a series of low angle peaks appear clearly in the range of $2\theta = 10-40°$ for the copper Cu/Ag(1:0) sample. This set of peaks is also present in the silver Cu/Ag(0:1) sample but is of much lower intensity (see inset) as compared to the Ag(111) diffraction. It is noted that these peaks are becoming more pronounced when the Cu to Ag feed ratio increases regularly in the series of MPACs. Such low angle peaks were detected in thiolated copper nanoclusters and attributed to superlattice diffractions.[23] Thus, the presence of these peaks suggests the formation of a regular arrangement of a 3D SAM of dodecanethiol on the series of MPAC samples prepared. In addition, since these peaks are more pronounced than the trend of increasing Cu-to-Ag feed ratios, it, thus, suggests that the surfaces of most of the MPACs are enriched with the copper component.

(B) Spectroscopic Analysis. *XPS Analysis.* Figure 3 depicts typical XPS spectra of the Cu/Ag MPACs over the full range of measurements as well as the individual elemental peaks. For all the samples prepared, the oxygen peak (~530 eV) is not detected. Table 1 summarizes the elemental XPS positions together with the respective percentage peak intensities. The absence of the oxygen peak, together with the absence of a charge-transfer shake-up satellite[28,29] of Cu, allows us to preclude any significant oxidation of the nanoclusters. This, thus, confirms an earlier conclusion that dodecanethiol 3D SAMs could form a good barrier layer to protect the metal cores from oxidation.[23] On the other hand, if we correlate the position of Cu $2p_{3/2}$ with the position of the $L_3M_{4,5}M_{4,5}$ Auger transition, the valence state of Cu was found to be between 0 and +1, confirming the chemisorption of 1-dodecanethiol onto the surface of the nanoclusters.[23]

The Ag $3d_{5/2}$ peaks for all the samples are detected at 368.1 eV (Table 1). This corresponds to a zero valence silver

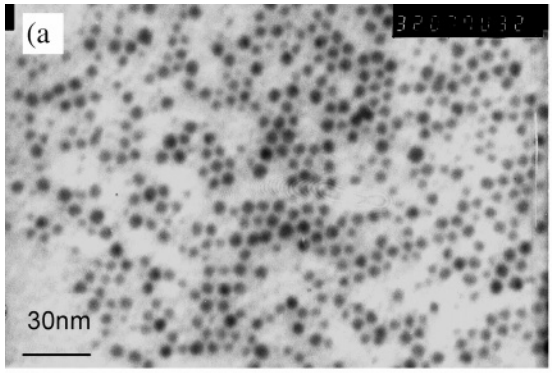
(a)
30nm

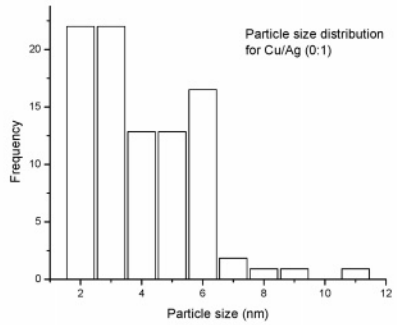
Particle size distribution for Cu/Ag (0:1)
Frequency
Particle size (nm)

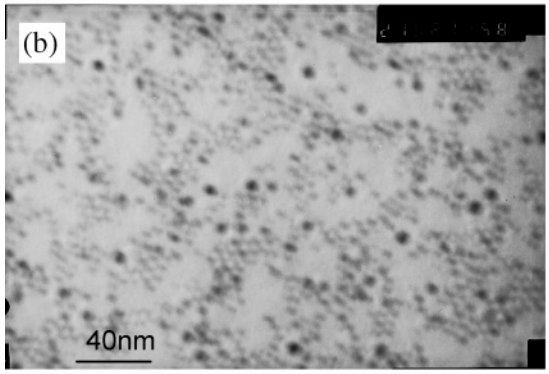
(b)
40nm

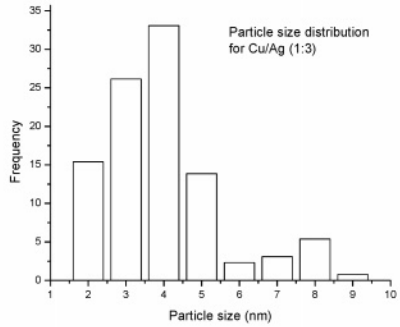
Particle size distribution for Cu/Ag (1:3)
Frequency
Particle size (nm)

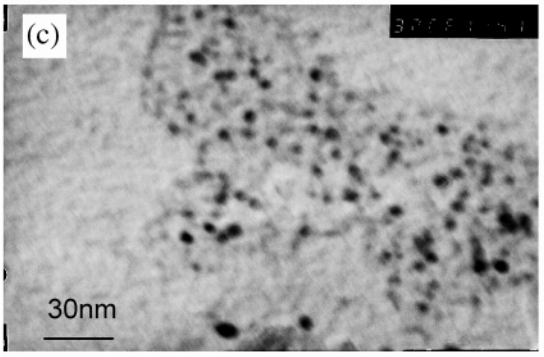
(c)
30nm

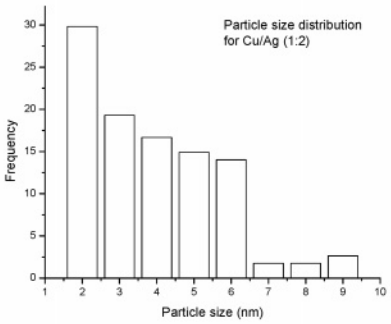
Particle size distribution for Cu/Ag (1:2)
Frequency
Particle size (nm)

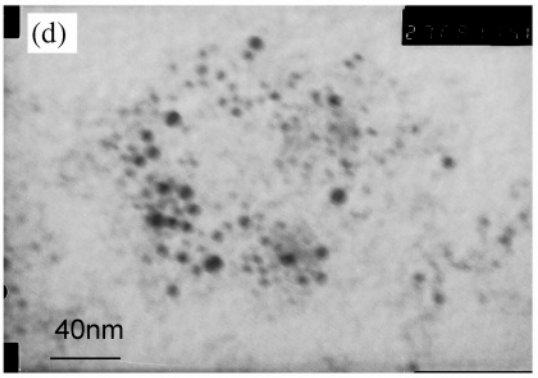
(d)
40nm

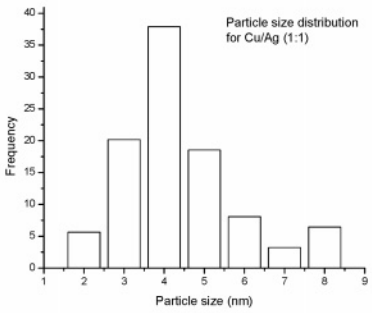
Particle size distribution for Cu/Ag (1:1)
Frequency
Particle size (nm)

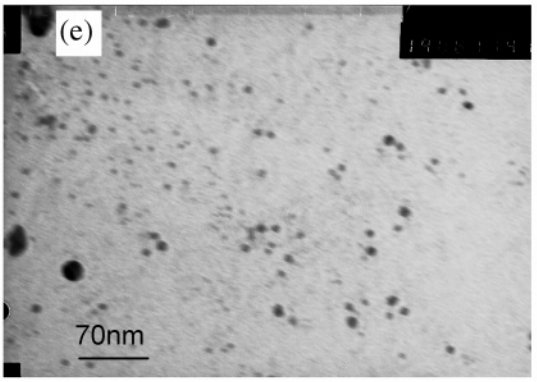
(e)
70nm

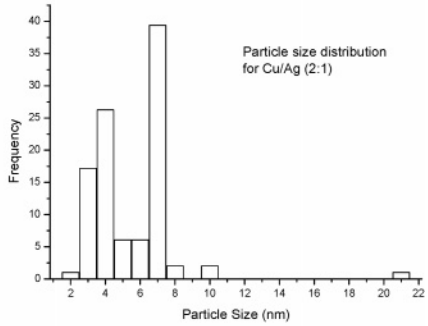
Particle size distribution for Cu/Ag (2:1)
Frequency
Particle Size (nm)

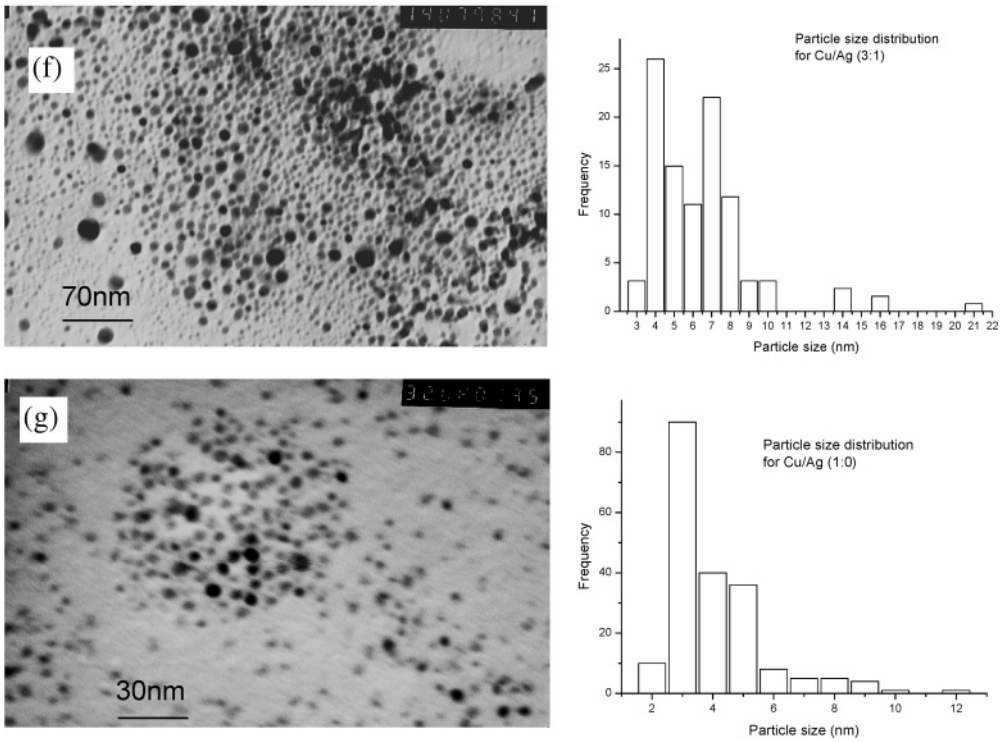

Figure 1. TEM images and size histograms of the alloy nanoclusters with various silver to copper feed ratios: (a) Cu/Ag(0:1); (b) Cu/Ag(1:3); (c) Cu/Ag(1:2); (d) Cu/Ag(1:1); (e) Cu/Ag(2:1); (f) Cu/Ag(3:1); (g) Cu/Ag(1:0).

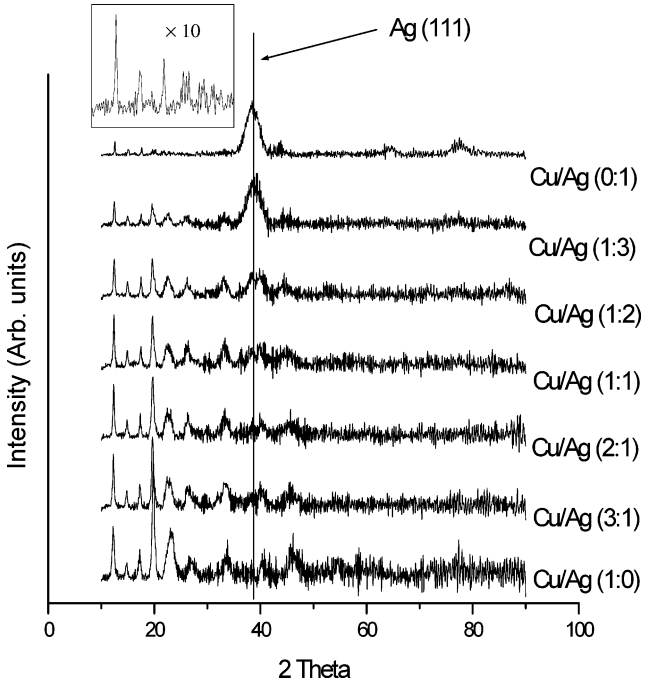

Figure 2. X-ray powder diffractograms of various Cu/Ag MPACs and their monometallic counterparts. The inset shows the expanded low angle region for the Cu/Ag(0:1) sample.

component, with the correct standard energy difference (6 eV) and relative theoretical intensity ratio between the $3d_{5/2}$ and $3d_{3/2}$ components. In the study of dodecanethiol-derivatized Ag/Au bimetallic nanoparticles, Han et al. made a similar observation for the Ag 3d and Au 4f peaks—they proposed that both silver and gold are present with net charges far below the resolution limit of the instrumental technique.[8] In other words, if 1-dodecanethiol molecules have chemisorbed onto the silver component in our samples, XPS will not be able to resolve the $\delta+$ charge of the Ag component.

There is only one type of sulfur species present in the nanoclusters, as suggested by XPS (Figure 3 and Table 1). In principle, the detection of a single sulfur species may point to the possibility of the MPACs having a core−shell structure. Nevertheless, Shon et al.,[15] Han et al.,[8] and Sandhyarani et al.[7] have also detected just one sulfur doublet for their alloy clusters. The XPS instrumental resolution, we believe, is not able to distinguish the different S species adsorbed onto silver and copper atoms, respectively. In general, the S $2p_{3/2}$ component at ∼162.3 eV compares very well with typical value of chemisorbed S species.[29]

A summary of the various elemental ratios obtained from the XPS peak area analysis, after sensitivity correction, is presented in Table 2. The C/S elemental ratios were found to be slightly higher than 12 for the chemisorbed 1-dodecanethiol, probably due to some carbonaceous contamination of the samples. On the other hand, the XPS Cu/Ag ratios are consistently higher than those given by elemental analysis (EA) for the copper-rich and the 1:1 samples. Since XPS results provide the surface composition while EA gives the bulk composition, these results, thus, confirm an enriched copper content on the surfaces of these MPACs. The total metal-to-S ratio, while being kept at 1:1 during preparation, is decreasing with an increasing copper composition in these MPACs. Interestingly, a relatively higher alkanethiol chain density has been reported on copper compared to a silver substrate in a 2D SAM study.[30] The trend of decreasing total metal-to-S ratio implies a higher density of SAM formation. This is, thus, consistent with the suggestion that the surfaces of these MPACs are increasingly enriched with the copper component.

Solid-State UV−Visible Spectroscopic Analysis. Figure 4 depicts the solid-state UV−visible absorption spectra of the MPACs, together with the monometallic silver and copper samples. While a broad silver surface plasmon peak at ∼450 nm is detected in the silver sample, the copper surface plasmon expected at ∼556 nm is absent in the monometallic copper

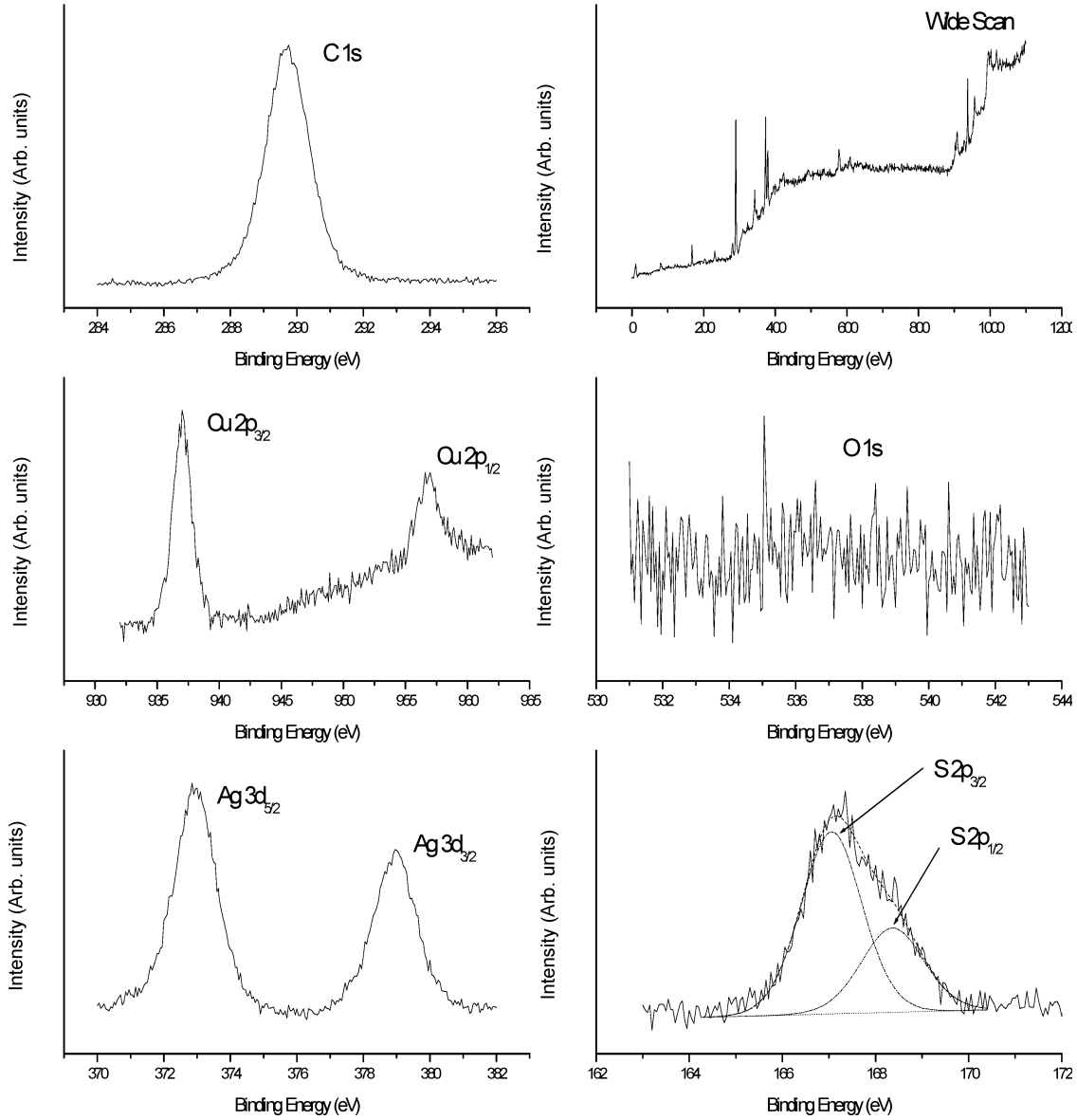

Figure 3. Representative XPS spectra of the MPACs, shown here for the Cu/Ag(1:1) sample.

TABLE 1: XPS Analysis of the Dodecanethiol-Protected Alloy and Monometallic Nanoclusters[a]

sample	C 1s	S $2p_{3/2}$	S $2p_{1/2}$	Cu $2p_{3/2}$	Cu $2p_{1/2}$	Ag $3d_{5/2}$	Ag $3d_{3/2}$
Cu/Ag(1:0)	284.8 (100)	162.4 (66.4)	163.6 (33.6)	932.3 (69.3)	952.1 (30.7)		
Cu/Ag(3:1)	284.8 (100)	162.3 (66.4)	163.6 (33.6)	931.8 (70.4)	951.6 (29.6)	368.1 (59.8)	374.1 (40.2)
Cu/Ag(2:1)	284.8 (100)	162.2 (66.5)	163.5 (33.5)	932.2 (71.7)	952.0 (28.3)	368.1 (59.6)	374.1 (40.4)
Cu/Ag(1:1)	284.8 (100)	162.2 (66.6)	163.5 (33.4)	932.2 (71.5)	951.9 (28.5)	368.1 (58.0)	374.1 (42.0)
Cu/Ag(1:2)	284.8 (100)	162.2 (66.8)	163.4 (33.2)	932.2 (71.7)	952.1 (28.3)	368.1 (58.9)	374.1 (41.1)
Cu/Ag(1:3)	284.8 (100)	162.2 (66.7)	163.4 (33.3)	931.8 (62.3)	951.6 (27.7)	368.1 (59.4)	374.1 (40.6)
Cu/Ag(0:1)	284.8 (100)	162.0 (66.6)	163.4 (33.4)			368.1 (59.7)	374.1 (40.3)

[a] Binding energy in eV. Numbers in parentheses are the relative percentage peak intensities.

samples. The absence of the copper plasmon peak has often been noted for a small cluster size with size dispersity,[23,25] and it is known that surface plasmon peaks of silver and gold are always much more intense than their copper counterparts.[31]

The silver plasmon peak is also observed in the silver-rich Cu/Ag(1:3) MPAC sample. On the other hand, a common peak at ~335−360 nm is clearly seen in all samples except the silver Cu/Ag(0:1) sample. It is noticed that this common peak is red-shifted consistently with a decreasing amount of copper present in the feed. We could not assign this peak with certainty at the moment, except knowing that the peak at ~335 nm may be attributed to a structure such as S−Cu−S.[32] The red shift in peak position seems to suggest interaction with the increasing amount of Ag atoms in the MPACs.

TABLE 2: Various Elemental Ratios Obtained from XPS and Cu/Ag Ratios from Elemental Analysis (EA)

sample	C/S	Cu/S	Ag/S	total metal/S	Cu/Ag	Cu/Ag from EA
Cu/Ag(1:0)	13.4	1.0		1.0		
Cu/Ag(3:1)	13.9	0.7	0.2	0.8	3.7	3.2
Cu/Ag(2:1)	13.4	0.6	0.3	0.9	2.4	2.2
Cu/Ag(1:1)	15.1	0.6	0.5	1.1	1.4	1.2
Cu/Ag(1:2)	15.3	0.5	0.6	1.2	0.8	0.8
Cu/Ag(1:3)	12.5	0.3	1.0	1.3	0.3	0.3
Cu/Ag(0:1)	12.6		1.0	1.0		

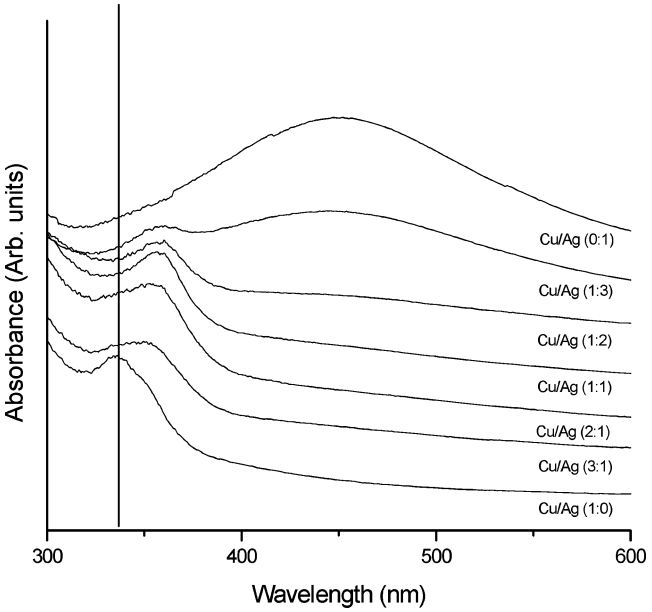

Figure 4. Solid UV−visible spectra of the various MPAC samples prepared, as compared to the monometallic silver and copper samples.

Transmission IR Analysis. Transmission IR spectroscopy has been found to be very useful in the study of 3D SAMs on nanoclusters.[6−8,23] In general, the overall features of the spectra will be similar to that of the neat molecules forming the SAM, since the structural integrity of the molecules is maintained upon chemisorption.[21] In the case of 1-dodecanethiol, the S−H stretching band at 2550−2600 cm^{-1} will disappear upon chemisorption. Important features in the IR spectra of the various MPACs (KBr pellets) are shown in Figure 5, compared with the case of neat 1-dodecanethiol.

It is observed that the CH_2 symmetrical (d^+) and asymmetrical (d^-) stretching bands of these samples appear at lower wavenumbers compared to those for 1-dodecanethiol (Figure 5a), and their progression bands appear clearly in Figure 5b. The d^+ and d^- CH_2 stretching vibrations are commonly used as an indicator for the degree of ordering (crystallinity) of the alkyl chains.[33] A shift to lower wavenumbers from those of the free thiol suggests that the chemisorbed thiol molecules are more ordered (adopt an all-trans zigzag conformation) on the surfaces of these MPACs. The well-resolved progression bands in the 1150−1400 cm^{-1} region have been assigned to the twisting−rocking (T_x) and wagging (W_x) progression bands. The appearance of these bands is also used as a strong indicator for the formation of a 3D SAM.[34]

Comparing the two monometallic samples, we have found that the progression peaks are much more prominent in the copper Cu/Ag(1:0) sample relative to the silver Cu/Ag(0:1) one. Interestingly, when the peak positions of the d^- and d^+ C−H stretching band are plotted against copper composition in Figure 6, an almost linear correlation is obtained in both cases. The shifts in IR peak position, thus, seem to be a useful parameter for the estimation of relative alloy components in these thiolated MPACs.

Obviously, such well-ordered thiol chains and progression bands may also suggest the formation of a multilayer stoichiometric thiolate compound during preparation. Nevertheless, the presence of a small broad peak at about 630 cm^{-1} in the IR spectrum, assignable to a C−S gauche peak and packing defects, suggested the formation of many defects in the samples. This has been noted as one of the differences between copper thiolated nanoclusters and its bilayer stoichiometric compound

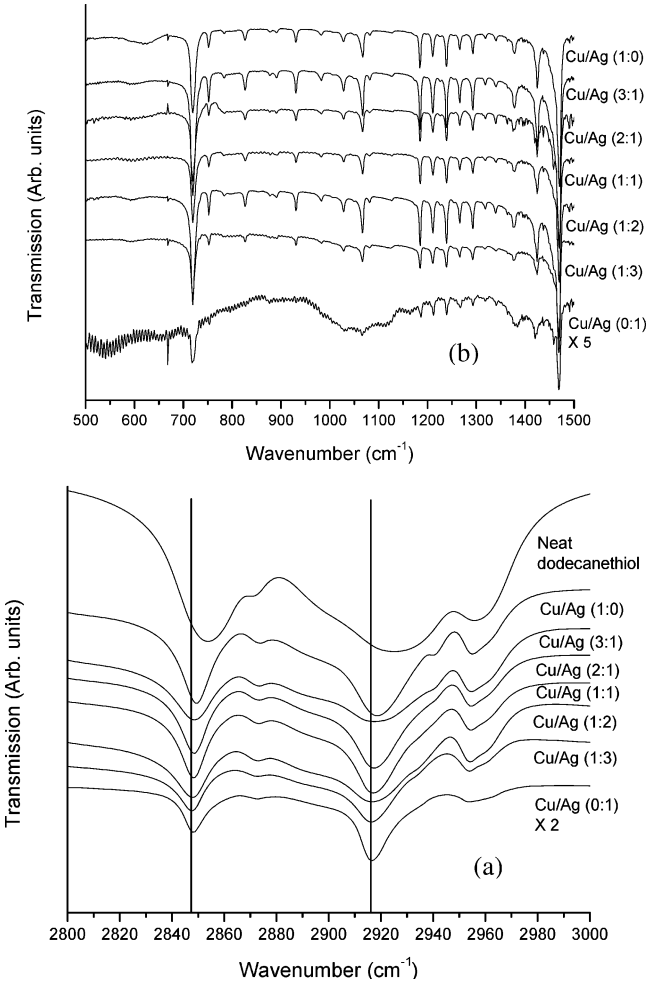

Figure 5. (a) Symmetrical and asymmetrical methylene C−H stretching modes of the prepared nanoclusters. The spectrum of neat dodecanethiol was included for comparison. (b) Progression peaks observed in the prepared nanoclusters, which are not observed in neat 1-dodecanethiol.

(see the Supporting Information), and it is also absent in the well-ordered silver thiolate stoichiometric analogue.[35]

^{13}C Cross-Polarization Magic Angle Spinning NMR. The solid-state cross-polarization magic angle spinning ^{13}C NMR (CPMAS ^{13}C NMR) spectra of the various MPACs are shown in Figure 7. For comparison, the ^{13}C NMR spectrum of 1-dodecanethiol monomer in $CDCl_3$ is included in the inset, together with the numbering of its carbon atoms on the right upper corner. Table 3 summarizes all the chemical shift values and the respective assignments.

In general, the resonances of carbons are shifted downfield with respect to neat 1-dodecanethiol upon chemisorption onto the alloy nanoclusters. Such a downfield shift has been attributed to conformationally more ordered dodecanethiol chains on the metal clusters.[22d] Expectedly, this downfield shift is much larger for carbons closer to the metal surface (i.e., C1), and it becomes smaller for carbons further away from the metal/sulfur interface. Indeed, the expected resonance for C1 vanishes once silver is added in the synthesis. Such a disappearance of the C1 resonance has also been reported for alkanethiol-protected gold nanoparticles and was attributed to very strong interaction between the sulfur atoms and the metal surface atoms.[22b,d,23]

Comparing the various MPACs and the monometallic clusters, differences in their chemical shift values are not significant but one can observe that there is a slight increase in peak width as the copper to silver feed ratio increases. Such a peak broadening

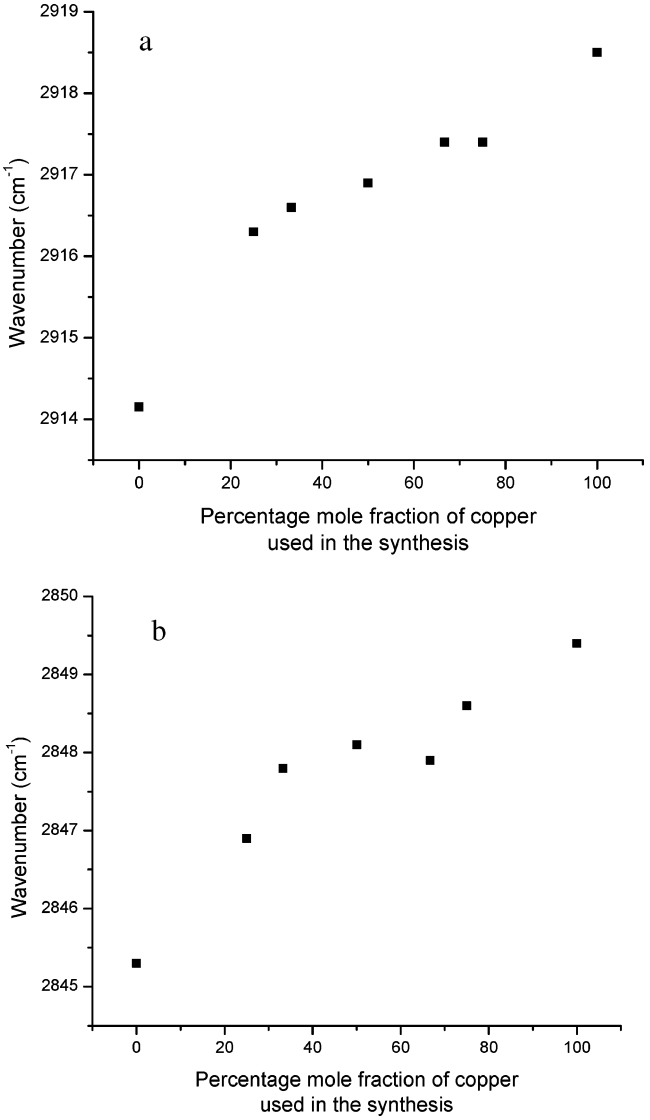

Figure 6. Plot of the copper feed composition in the MPACs versus the IR peak positions of (a) asymmetric C−H stretching and (b) symmetric C−H stretching.

can be verified most clearly from the gradual disappearance of the shoulder peak at ~35 ppm from Cu/Ag(0:1) to Cu/Ag(1:0). Such peak broadening may arise as a result of the fast spin relaxation from mutual dipolar interaction among the ordered chains.[23] Thus, the increase in peak width with increasing copper content seems to suggest stronger dipolar chain−chain interactions and a more ordered chain arrangement in the copper-rich samples. It is noteworthy that the peak profiles of most MPACs are closer to that of the copper Cu/Ag(1:0) sample, and this again points to the possible surface enrichment with the copper component.

(C) Thermal Analysis. *Thermogravimetric Analysis (TGA).* Figure 8 shows the TGA results of the various thiolated MPACs, for which a transition is seen for the desorption of dodecanethiol from the cluster surface. The desorption temperature and the percentage weight loss are tabulated in Table 4.

From Figure 8 and Table 4, we observe that the monometallic copper Cu/Ag(1:0) sample has the highest desorption temperature and percentage weight loss, while the silver Cu/Ag(0:1) sample has the lowest. This observation, thus, confirms that a higher coverage of dodecanethiol is present on the copper clusters. On the other hand, the desorption temperatures of the series of MPAC samples are similar but their percentage weight losses are increasing with increasing copper feed ratio. Since

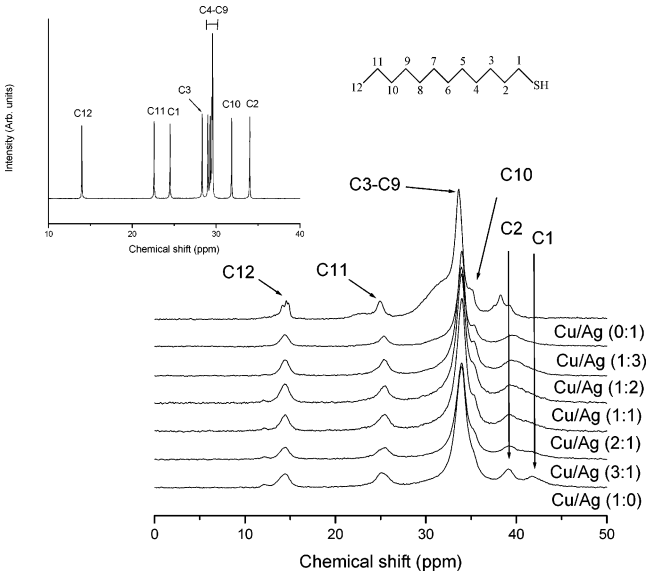

Figure 7. CPMAS ^{13}C NMR spectra for the various MPACs and the monometallic silver and copper nanoclusters. The spectrum of 1-dodecanethiol is included for comparison with the carbon assignment and numbering shown at the right upper corner.

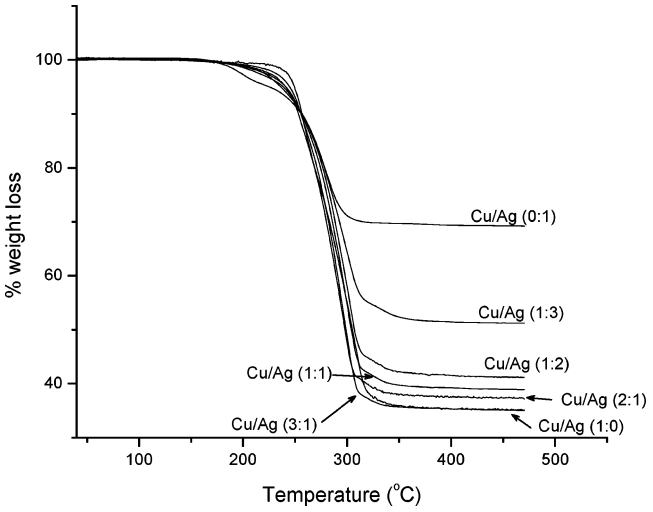

Figure 8. Thermogravimetric graphs of the various alloy and monometallic nanoclusters.

TABLE 3: Chemical Shift Values (δ, ppm) and Assignments of the Various Carbon Sites

	δ (ppm)				
	C1	C2	C3−C10	C11	C12
1-dodecanethiol	24.5	34.0	28.3−31.8	22.6	14.0
Cu/Ag(1:0)	41.5	38.9	31.3−35.6	25.0	14.3
Cu/Ag(3:1)		38.9	31.6−35.6	25.4	14.4
Cu/Ag(2:1)		38.9	32.7−35.5	25.3	14.4
Cu/Ag(1:1)		39.1	32.0−35.0	25.4	14.3
Cu/Ag(1:2)		39.2	32.3−35.0	25.2	14.3
Cu/Ag(1:3)		39.3	32.5−35.1	25.2	14.3
Cu/Ag(0:1)		38.0	30.0−35.0	24.8	14.5

the average particle size for all the MPACs is quite similar, this result implies an increasing coverage of dodecanethiol on the alloy clusters with increasing copper content. The increase is not linear; nevertheless, a plot in Figure 9 suggests that the extent of weight loss is becoming less significant when the Cu to Ag feed ratio reaches 2:1 and beyond. Thus, it seems that the enrichment of the copper component on the surfaces of the MPACs has also led to a higher coverage of dodecanethiol on the surfaces.

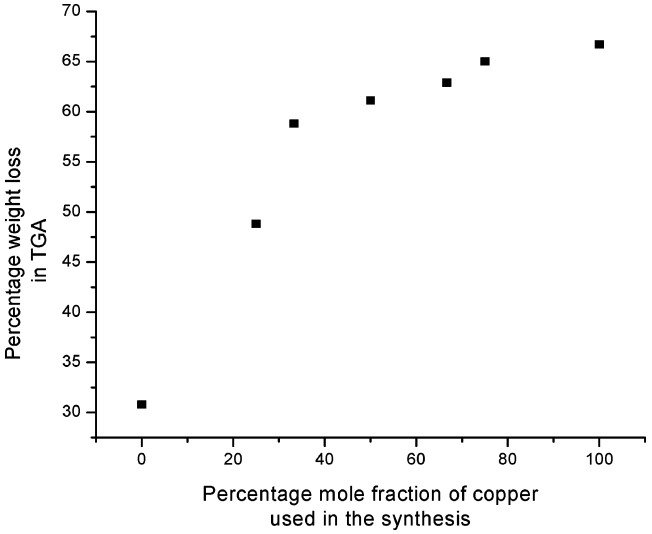

Figure 9. Graph of the percentage weight loss found in TGA versus the percentage mole fraction of copper feed.

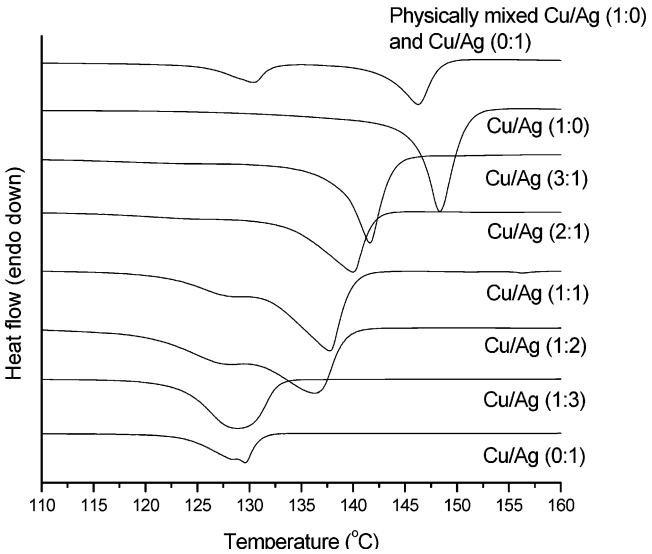

Figure 10. DSC endotherms of the various MPACs.

TABLE 4: Desorption Onset and Percentage Weight Loss for the Prepared Nanoclusters

sample	desorption temperature (°*C*)	percentage weight loss (%)
Cu/Ag(0:1)	241.2	30.8
Cu/Ag(1:3)	253.2	48.8
Cu/Ag(1:2)	262.2	58.8
Cu/Ag(1:1)	260.3	61.1
Cu/Ag(2:1)	254.4	62.9
Cu/Ag(3:1)	258.2	65.0
Cu/Ag(1:0)	263.8	66.7

Differential Scanning Calorimetry (DSC). Figure 10 illustrates the DSC heating curves for the samples from 110 to 160 °C. The respective transition points and enthalpies of the endotherms are listed in Table 5. For comparison, a 1:1 physically mixed monometallic sample was measured. Expectedly, two distinct DSC peaks are detected in this mixture, with characteristics corresponding well to those found in the respective monometallic Cu/Ag(1:0) and Cu/Ag(0:1) components. Thus, the distinct DSC peak profiles of the MPACs clearly confirm that bimetallic alloys have been formed indeed.

Comparing along the series of MPACs, the melting points and enthalpies are found to increase quite regularly with the copper to silver feed ratios. These endotherms in DSC are often attributed to disruption of the interdigitation between 3D SAMs of thiols on neighboring nanoclusters.[23] It has been suggested that the melting point (relating to the degree of interdigitation) and melting enthalpy (relating to the amount of interdigitation) exhibited in a DSC endotherm provide an indirect measure of the population of trans conformers present in the sample.[22b,e] The results in Table 5, thus, clearly suggest that the degree and the amount of interdigitation increase with increasing copper to silver feed ratio, and this implies that the population of trans conformations is also increasing in the same order.

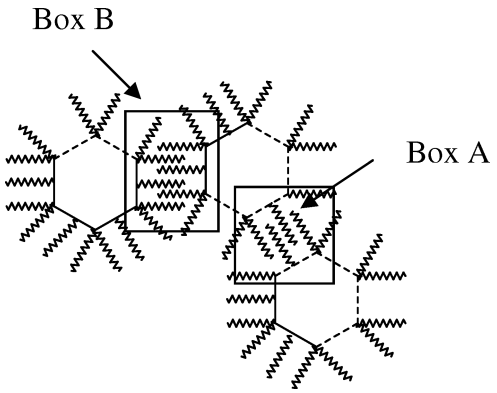

Figure 11. Cartoon to illustrate the interdigitation of alkyl chains on different sites of the alloy surfaces. Surfaces marked with dotted lines are dominated by silver atoms, while those with solid lines are enriched with copper atoms.

TABLE 5: Melting Points and Melting Enthalpies for the MPACs and the Physically Mixed Sample

sample	melting point (°**C**)	melting enthalpy (J/g)
Cu/Ag(0:1)	129.6	29.5
Cu/Ag(1:3)	128.9	79.6
Cu/Ag(1:2)	136.3	114.3
Cu/Ag(1:1)	137.7	123.1
Cu/Ag(2:1)	140.0	114.7
Cu/Ag(3:1)	141.6	141.8
Cu/Ag(1:0)	148.4	130.8
physically mixed sample	130.4, 146.3	15.3, 32.9

On closer inspection, we notice that the Cu/Ag(1:3) sample has a similar melting point to that of the silver Cu/Ag(0:1) sample, although the melting enthalpy is much higher for the former. We believe this indicates that the Cu/Ag(1:3) sample, being silver-rich, has its surface occupied by more silver atoms. Interestingly, DSC endotherms for Cu/Ag(1:2) and Cu/Ag(1:1) samples were also seen to show a shoulder at about the same temperature, ~130 °C, as that for the Cu/Ag(1:3) main peak. This shoulder was not observed when the copper to silver feed ratio reached 2:1 and beyond. The presence of two melting transitions in these two samples is very interesting and may be taken to imply two different adsorption sites on the MPACs. We, thus, propose to attribute the peak at ~130 °C to the melting of interdigitated dodecanethiol chains adsorbed onto a silver-rich surface (shown as box A in Figure 11), while the peak at the higher temperature (136−142 °C for most MPACs) is attributed to the melting of interdigitated dodecanethiol chains adsorbed onto a copper-rich surface (shown as box B in Figure 11). The relative peak area of these two DSC peaks could, thus, provide an indirect measure of the surface properties of these bimetallic MPACs.

Thus, during the growth of MPACs, galvanic exchange occurs and Cu atoms will move toward the surface of the growing crystals and intercalate with the surface Ag atoms. Our thermal analysis suggested that the surface enrichment occurs in a heterogeneous manner, especially in MPACs with intermediate

feed ratios. In the case of the silver-rich Cu/Ag(1:3) sample, we believe the amount of Cu atoms available for intercalation was limited and, thus, the surface of the nanoclusters is still dominated by Ag atoms. By increasing the amount of copper used in the feed, the surface is progressively enriched with copper atoms and, hence, the surface properties, as well as the 3D SAMs formed, will be approaching those of the copper Cu/Ag(1:0) sample.

Conclusion

We demonstrated in this paper the synthesis of thiolated copper/silver bimetallic alloy nanoclusters via a liquid-phase method. Our results show that spherical bimetallic nanoparticles of ~4−6 nm are produced but that a galvanic exchange reaction has taken place such that surfaces of the prepared clusters are enriched with the less noble metal copper atoms. This is clearly supported by the behavior of the dodecanethiol 3D SAMs from XRD, XPS, FTIR, and NMR analysis. Our finding is important to future applications of bimetallic alloys, since the surface-active component is expected to play a major role in applications such as catalysis. The surface behavior was found to still be dominated by silver atoms, however, when the amount of copper atoms is limited to a Cu/Ag feed ratio of 1:3.

In addition, we have provided clear evidence for the interdigitation of the 3D SAM chains between neighboring alloy clusters. It does seem that most of the dodecanethiol chains will adopt an extended all-trans conformation to allow them to pack densely on the alloy clusters, especially on the copper-rich surfaces. Upon heating, some of the all-trans conformations are gradually disrupted and a phase transition point (T_m) can be observed in DSC. Interestingly, two slightly different transitions have been detected that could be attributed to the interdigitation of SAMs adsorbed onto two different surfaces (i.e., copper- or silver-rich). This observation is interesting as it clearly illustrates the heterogeneous segregation of the metallic components on the alloy surfaces, for samples prepared with intermediate metal feed ratios.

Acknowledgment. This research work is supported by a National University of Singapore research grant (Grant Number: R-143-000-123-112). We thank Dr. Liu Chenmin for her assistance in extending the TEM analysis.

Supporting Information Available: Comparison between the copper dodecanthiolate stoichiometric bilayer compound and the dodecanethiolated copper nanoclusters: synthesis, TEM, FTIR, NMR, TGA, and DSC data. This material is available free of charge via the Internet at http://pubs.acs.org.

References and Notes

(1) (a) Sinfelt, J. H. *J. Catal.* **1973**, *29*, 308. (b) Sinfelt, J. H. *Acc. Chem. Res.* **1987**, *20*, 134.

(2) (a) Toshima, N. *J. Macromol. Sci., Chem.* **1990**, *A27*, 1225. (b) Toshima, N.; Yonezawa, T. *New J. Chem.* **1998**, 1179.

(3) Harikumar, K. R.; Ghosh, S.; Rao, C. N. R. *J. Phys. Chem. A* **1997**, *101*, 536.

(4) (a) Henglein, A.; Brancewicz, C. *Chem. Mater.* **1997**, *9*, 2164. (b) Michaelis, M.; Henglein, A.; Mulvaney, P. *J. Phys. Chem.* **1994**, *98*, 6212. (c) Mulvaney, P.; Giersig, M.; Henglein, A. *J. Phys. Chem.* **1993**, *97*, 7061.

(5) Remita, H.; Khatouri, J.; Treguer, M.; Amblard, J.; Belloni, J. *Z. Phys. D* **1997**, *40*, 127.

(6) Hostetler, M. J.; Zhong, C. J.; Yen, B. K. H.; Anderegg, J.; Gross, S. M.; Evans, N. D.; Porter, M.; Murray, R. W. *J. Am. Chem. Soc.* **1998**, *120*, 9396.

(7) Sandhyarani, N.; Predeep, T. *Chem. Mater.* **2000**, *12*, 1755.

(8) Han, S. W.; Kim, Y.; Kim, K. *J. Colloid Interface Sci.* **1998**, *208*, 272.

(9) Schimid, G. *Clusters and Colloids*; VCH: Weinheim, Germany, 1994.

(10) Kariuki, N. N.; Luo, J.; Maye, M. M.; Hassan, S. A.; Menard, T.; Naslund, H. R.; Lin, Y. H.; Engelhard, C. M.; Chong, C. J. *Langmuir* **2004**, *20*, 11240.

(11) Rivas, L.; Sanchez-Cortes, S.; Gracia-Ramos. J. V.; Morcillo, G. *Langmuir* **2000**, *16*, 9722.

(12) Srnová-Sloufová, I.; Lednický, F.; Gemperle, A.; Gemperlová, J. *Langmuir* **2000**, *16*, 9928.

(13) Freeman, R. G.; Hommer, M. B.; Grabar, K. C.; Jackson, M. A.; Natan, M. J. *J. Phys. Chem.* **1996**, *100*, 718.

(14) Chen, Y. H.; Nickel, U. *J. Chem. Soc., Faraday Trans.* **1993**, *89*, 2479.

(15) Shon, Y. S.; Dawson, G. B.; Porter, M.; Murray, R. W. *Langmuir* **2002**, *18*, 3880.

(16) Papavassiliou, G. C. *J. Phys. F: Met. Phys.* **1976**, *6*, L103.

(17) Takeuchi, Y,; Ida, T.; Kimura, K. *J. Phys. Chem. B* **1997**, *101*, 1322.

(18) (a) Hodak, J. H.; Henglein, A.; Giersig, M.; Hartland, G. V. *J. Phys. Chem. B* **2000**, *104*, 11708. (b) Hodak, J. H.; Henglein, A.; Hartland, G. V. *J. Phys. Chem. B* **2000**, *104*, 9954.

(19) Abid, J. P.; Girault, H. H.; Brevet, P. F. *Chem. Commun.* **2001**, 829.

(20) Chen, Y. H.; Yeh, C. S. *Chem. Commun.* **2001**, 371.

(21) Love, J. C.; Estroff, L. A.; Kriebel, J. K.; Nuzzo, R. G.; Whitesides, G. M. *Chem. Rev.* **2005**, *105*, 1103.

(22) (a) Brust, M.; Walker, M.; Bethell, D.; Schiffrin, D. J.; Whyman, M. *J. Chem. Soc., Chem. Commun*. **1994**, 801. (b) Terrill, R. H.; Postlethwaite, T. A.; Chen, C. H.; Poon, C. D.; Terzis, A.; Chen, A.; Hutchison, J. E.; Clark, M. R.; Wignall, G.; Londono, J. D.; Superfine, R.; Falvo, M.; Johnson, C. S., Jr.; Samulski, E. T.; Murray, R. W. *J. Am. Chem. Soc.* **1995**, *117*, 12537. (c) Badia, A.; Demers, L.; Dickinson, L.; Morin, F. G.; Lennox, R. B.; Reven, L. *J. Am. Chem. Soc.* **1997**, *119*, 11104. (d) Badia, A.; Gao, W.; Singh, S.; Dmers, L.; Cuccia, L.; Reven, L. *Langmuir* **1996**, *12*, 1262. (e) Badia, A,; Singh, S.; Demers, L.; Cuccia, L.; Brown, G. R.; Lennox, R. B. *Chem.—Eur. J.* **1996**, *2* (3), 359.

(23) Ang, T. P.; Wee, T. S. A.; Chin, W. S. *J. Phys Chem. B* **2004**, *108*, 11101.

(24) (a) Espinet, P.; Lequerica, M. C.; Martín-Alvarez, J. M. *Chem.—Eur. J.* **1999**, *7*, 1982. (b) Sandhyarani, N.; Pradeep, T. *J. Mater. Chem.* **2001**, 1294.

(25) Chen, S. W.; Sommers, J. M. *J. Phys. Chem. B* **2001**, *105*, 8816.

(26) Murthy, S.; Bigioni, T. P.; Wang, Z. L.; Khoury, J. T.; Whetten, R. L. *Mater. Lett.* **1997**, *30*, 321.

(27) Dhas, N. A.; Raj, C. P.; Gedanken, A. *Chem. Mater.* **1998**, *10*, 1446.

(28) (a) Mclntyre, N. S.; Cook, M. G. *Anal. Chem.* **1975**, *47*, 2208. (b) Shoen, G. *Surf. Sci*. **1973**, *35*, 96. (c) Larson, P. E. *J. Electron Spectrosc. Relat. Phenom.* **1974**, *4*, 213.

(29) (a) Bensebaa, F.; Zhou, Y.; Deslandes, Y.; Kruus, E.; Ellis, T. H. *Surf. Sci.* **1998**, *405*, L472. (b) Moulder, J. F.; Stickle, W. F.; Sobol, D. E.; Bomben, K. D. In *Handbook of X-ray Photoelectron Spectroscopy*; Chastain, J., Ed.; Perkin-Elmer Corporation: Minnesota, 1992.

(30) Laibinis, P. E.; Whitesides, G. M.; Allara, D. L.; Tao, Y.-T.; Parikh, A. N.; Nuzzo, R. G. *J. Am. Chem. Soc.* **1991**, *113*, 7152.

(31) Creighton, J. A.; Eadon, D. G. *J. Chem. Soc., Faraday Trans.* **1991**, *87*, 3881.

(32) Fujisawa, K.; Imai, S.; Kitajima, N.; Moro-oka, Y. *Inorg. Chem.* **1998**, *37*, 168.

(33) (a) Bradley, J. S. In *Clusters and colloids*; Schmid, G., Ed.; VCH: Weinhein, Germany, 1994; pp 459−544. (b) Edwards, P. P. *Mater. Res. Soc. Symp. Proc.* **1992**, *272*, 311.

(34) (a) Hostetler, M. J.; Stokes, J. J.; Murray, R. W. *Langmuir* **1996**, *12*, 3604. (b) Nuzzo, R. G.; Dubois, L. H.; Allara, D. L. *J. Am. Chem. Soc.* **1990**, *112*, 558.

(35) Sandhyarani, N.; Anthony, M. P.; Selvam, G. P.; Pradeep, T. *J. Chem. Phys.* **2000**, *113*, 9794.